arXiv:0902.1701v1 [astro-ph.HE] 10 Feb 2009

Radio polarimetry signatures of strong magnetic turbulence in Supernova Remnants

Wendy Stroman

Department of Physics and Astronomy, Iowa State University, Ames, IA 50011

and

Martin Pohl

Department of Physics and Astronomy, Iowa State University, Ames, IA 50011

mkp@iastate.edu

ABSTRACT

We discuss the emission and transport of polarized radio-band synchrotron radiation near the forward shocks of young shell-type supernova remnants, for which X-ray data indicate a strong amplification of turbulent magnetic field. Modeling the magnetic turbulence through the superposition of waves, we calculate the degree of polarization and the magnetic polarization direction which is at 90° to the conventional electric polarization direction. We find that isotropic strong turbulence will produce weakly polarized radio emission even in the absence of internal Faraday rotation. If anisotropy is imposed on the magnetic-field structure, the degree of polarization can be significantly increased, provided internal Faraday rotation is inefficient. Both for shock compression and a mixture with a homogeneous field, the increase in polarization degree goes along with a fairly precise alignment of the magnetic-polarization angle with the direction of the dominant magnetic-field component, implying tangential magnetic polarization at the rims in the case of shock compression. We compare our model with high-resolution radio polarimetry data of Tycho's remnant. Using the absence of internal Faraday rotation we find a soft limit for the amplitude of magnetic turbulence, $\delta B \lesssim 200\ \mu$G. The data are compatible with a turbulent magnetic field superimposed on a radial large-scale field of similar amplitude, $\delta B \simeq B_0$. An alternative viable scenario involves anisotropic turbulence with stronger amplitudes in the radial direction, as was observed in recent MHD simulations of shocks propagating through a medium with significant density fluctuations.

Subject headings: acceleration of particles, cosmic rays, methods: numerical, shock waves, supernova remnants, turbulence

1. Introduction

The origin of Galactic cosmic rays and the mechanisms of their acceleration are among the most challenging problems in astrophysics. Shell-type supernova remnants (SNR) have long been thought to be the sources of cosmic rays, primarily through acceleration at their powerful forward shocks. Particle acceleration at collisionless shocks is intrinsically efficient (e.g. Kang & Jones 2005) and arises from pitch-angle scattering in the plasma flows that have systematically different velocities upstream and downstream of the shock (Bell 1978). Detailed studies show that the acceleration efficiency and the resulting spectra depend on the orientation angle of the magnetic field and on the amplitude and characteristics of magnetic turbulence near the shock (e.g. Giacalone & Jokipii 1996; Malkov & Diamond 2001; Giacalone 2005; Bykov & Toptygin 2005), part of which is self-generated. The amplitude of the turbulence also sets the scale for the maximum energy to which a remnant may accelerate particles. For typical interstellar magnetic field values, SNRs can at best accelerate particles to 10^{15} eV, where the cosmic-ray spectrum shows a break known as the *knee* (Lagage & Cesarsky 1983a,b). If the cosmic rays would drive a turbulent magnetic field to an amplitude much larger than the homogeneous interstellar field (Lucek & Bell 2000; Bell & Lucek 2001), particle acceleration may be faster and extend to higher energies (Vladimirov et al. 2006).

Bell (2004) found that, rather than resonant Alfvén waves, the current carried by drifting cosmic rays should efficiently excite non-resonant, nearly purely growing modes of magnetic turbulence on spatial scales much smaller than the cosmic-ray Larmor radius. MHD simulations that assume the cosmic-ray current to be constant (Bell 2004, 2005; Zirakashvili et al. 2008; Reville et al. 2008) indeed indicate a strong magnetic-field amplification following an approximately isotropic plasma filamentation in the non-linear stage. On the other hand, recent kinetic simulations suggest that the amplitude of the field perturbations saturates at approximately the amplitude of the homogeneous upstream field on account of nonlinear backreactions (Niemiec et al. 2008). Density fluctuations in the upstream region will also distort the shock, leading to turbulent magnetic-field growth downstream (Balsara et al. 2001; Giacalone & Jokipii 2007; Zirakashvili & Ptuskin 2008).

While its micro-physics is not fully understood, magnetic-field amplification is observationally required to explain that a large fraction of the non-thermal X-ray emission on the rims of young SNRs is concentrated in narrow filaments (e.g. Hughes 2000; Gotthelf et al. 2001; Hwang et al. 2002; Bamba et al. 2003, 2005). These filaments can be interpreted either as limited by rapid energy losses of the radiating electrons (Vink & Laming 2003; Bamba et al. 2003) or, alternatively, as caused by rapid damping of strong magnetic turbulence downstream of the SNR shock (Pohl et al. 2005). Both interpretations require

magnetic-field amplification, and the turbulently amplified field is expected to have a small wavelength. A very strong magnetic field is also suggested by time-variability of patches of non-thermal X-ray emission near the forward shock of SNR RX J1713-3946 (Uchiyama et al. 2007), although observational limits to the radio emission of secondary electrons (Huang & Pohl 2008) and the cosmic-ray e/p ratio in general (Katz & Waxman 2008) indicate that we could observe just the build-up and decay of a magnetic structure (e.g. Butt et al. 2008; Bykov et al. 2008).

Because of its role in particle acceleration it is of paramount importance to understand the properties of strong magnetic turbulence near the forward shocks of SNRs. A significant uncertainty in our interpretations arises from the unknown spatial distribution of the strong, turbulent magnetic field. The properties of the turbulent magnetic field can be traced through synchrotron intensity fluctuations (e.g. Cho & Lazarian 2002) or through polarimetry. Here we present a search for signatures of such turbulence in polarized radio synchrotron emission. For that purpose we create parametrized models of magnetic turbulence and calculate the emission and transport of linearly polarized synchrotron radiation through the turbulent downstream medium, including the effects of Faraday rotation. The results are compared with published radio polarimetry data of Kepler's SNR (SN 1604) (DeLaney et al. 2002) and Tycho's SNR (SN 1572) (Dickel et al. 1991).

Since the degree of linear polarization and the polarization angle depend mainly on the structure of the turbulent magnetic field, our results are very generic and can be widely applied. The amplitude of the magnetic field enters only through a scaling parameter that describes the extent of depolarization through Faraday rotation.

2. The model

2.1. Parametrization of the turbulent magnetic field

A turbulent magnetic field can be constructed via superposition of many magnetic waves with random orientation. A single magnetic wave carries a magnetic-field vector of the form

$$\mathbf{B} = \mathbf{B}_0 \sin\left(\mathbf{k} \cdot \mathbf{x}\right) \tag{1}$$

and is assumed to fill all space. In order to ensure that $\nabla \cdot \mathbf{B} = 0$, we choose magnetic-field components of the form (Giacalone & Jokipii 1994; Niemiec & Ostrowski 2006)

$$\begin{aligned} B_x &= B_{0,x} \sin\left(k_y y + k_z z + \sigma_x\right) \\ B_y &= B_{0,y} \sin\left(k_x x + k_z z + \sigma_y\right) \\ B_z &= B_{0,z} \sin\left(k_x x + k_y y + \sigma_z\right), \end{aligned} \tag{2}$$

where the σ_i terms denote randomly generated phase shifts. The projections of the wavevector $\mathbf{k}$ are:

$$\begin{aligned} k_x &= k \sin\theta \cos\eta \\ k_y &= k \sin\theta \sin\eta \\ k_z &= k \cos\theta \end{aligned} \tag{3}$$

where the angles θ and η are randomly selected to generate isotropic turbulence. The wavenumber k is randomly generated with uniform distribution in $\ln k$, such that $2\pi \times 10^{-3} \leq k \leq 4\pi \times 10^{-1}$ inverse cell units. This allows a range of wavelengths between 5 and 1000 cell units, or $20 - 4000$ periods along the line of sight. The amplitude of the magnetic wave follows

$$B_0(k) = B_0(k_{min}) \left[\frac{k}{k_{min}}\right]^{\frac{1-q}{2}} \qquad k_{min} \leq k \leq k_{max}, \tag{4}$$

where we consider two possible values for the power-law index, q. For a Kolmogorov spectrum $q = 5/3$ and for a flat spectrum $q = 1$. For a model with a Kolmogorov spectrum, the rms magnetic amplitude is $\delta B = \sqrt{\langle B_{x'}^2 + B_{y'}^2 + B_{z'}^2 \rangle} \approx 10\mu$G, while a flat-spectrum model results in $\delta B \approx 20\mu$G. The flat-spectrum models involve more small-scale fluctuations than do the Kolmogorov models. We do not know the true shape of the turbulence spectrum in SNRs, but comparing the results for the two magnetic-field models permits at least a qualitative estimate of the expected results for arbitrary spectra.

The projections of the magnetic-field vector are determined in the same way as for $\mathbf{k}$:

$$\begin{aligned} B_{0,x} &= B_0 \sin\zeta \cos\xi \\ B_{0,y} &= B_0 \sin\zeta \sin\xi \\ B_{0,z} &= B_0 \cos\zeta, \end{aligned} \tag{5}$$

except that ζ and ξ are new angles, still randomly generated such that $-1 \leq \cos\zeta \leq 1$ and $0 \leq \xi \leq 2\pi$. It is straightforward to develop a turbulent magnetic field from the superposition of 1000 waves by summing each component as follows

$$B_{x,tot} = \sum_{i=1}^{1000} B_{0x,i} \sin\left(k_{y,i}\, y + k_{z,i}\, z + \sigma_{x,i}\right). \tag{6}$$

While it is important to ensure that $\nabla \cdot \mathbf{B} = 0$ for each wave, the final magnetic field components must also fluctuate along all three coordinate axes, otherwise there would be no field reversals along the line of sight and hence no turbulent Faraday rotation. Therefore, we rotate the coordinate system by 45 degrees around each axis, thus changing the coordinates (x, y, z) to (x', y', z') via

$$\mathbf{x}' = \frac{1}{2\sqrt{2}} \begin{pmatrix} 1-\sqrt{2} & 1+\sqrt{2} & -\sqrt{2} \\ -1-\sqrt{2} & -1+\sqrt{2} & \sqrt{2} \\ \sqrt{2} & \sqrt{2} & 2 \end{pmatrix} \mathbf{x} \tag{7}$$

The rows of the transformation matrix give the unit vectors of the primed coordinate system, $\mathbf{e_{x'}}$, $\mathbf{e_{y'}}$, and $\mathbf{e_{z'}}$, and the columns contain the unit vectors of the old coordinate system, $\mathbf{e_x}$, $\mathbf{e_y}$, and $\mathbf{e_z}$. The projections of the magnetic-field vector on the new coordinate axes are

$$B_{x'} = \mathbf{e_{x'}} \cdot (B_{x,tot}, B_{y,tot}, B_{z,tot}) \tag{8}$$

and analogously for $B_{y'}$ and $B_{z'}$. Here Eq. 6 is written in term of the primed coordinates

$$B_{x,tot} = \sum_{i=1}^{1000} B_{0x,i} \sin\left(k_{y,i}\, \mathbf{e_y} \cdot \mathbf{x'} + k_{z,i}\, \mathbf{e_z} \cdot \mathbf{x'} + \sigma_{x,i}\right). \tag{9}$$

and correspondingly for $B_{y,tot}$ and $B_{z,tot}$. It is straightforward to see that $B_{x'}$ now depends on x' etc.

In the primed coordinate system, a three-dimensional grid is defined with size 20x20x20000 cells or 50x50x20000 cells. The longest dimension (20000 cells) corresponds to the line of sight, while the other two dimensions are in the plane of the sky.

2.2. Transport of polarized radio emission

We are interested in modeling the observed polarized radio emission near the rims of the remnant, where any signatures of the possibly warped contact discontinuity can be ignored. Figure 1 shows a sketch of the geometry. Radio observations of SNRs suggest that the synchrotron intensity, and therefore the spectrum of radiating electrons, follows a power law $j_\nu \propto \nu^{-\alpha}$ (Green 2001). The emissivity also depends on the perpendicular component of the magnetic field in the emission region:

$$j_\nu = K\,(\alpha)\; B_\perp^{\alpha+1}\, \nu^{-\alpha} \qquad \text{with } B_\perp^2 = B_{x'}^2 + B_{y'}^2, \tag{10}$$

where $K(\alpha)$ is a constant depending on the density of relativistic electrons (Rybicki & Lightman 1979). For an isotropic ensemble of electrons the synchrotron emissivity has a degree of linear polarization

$$p = \frac{\alpha + 1}{\alpha + 5/3} \tag{11}$$

which is independent of frequency (Le Roux 1961). For typical values of $\alpha = 0.5$ or $\alpha = 0.7$ the initial degree of linear polarization is 70% and 72%, respectively.

Radiotelescopes typically measure the electric-field direction of a linearly polarized wave, which reflects the direction of acceleration of the radiating electron. The *electric*-polarization angle is then rotated by 90° to obtain the *magnetic*-polarization angle, which reflects the

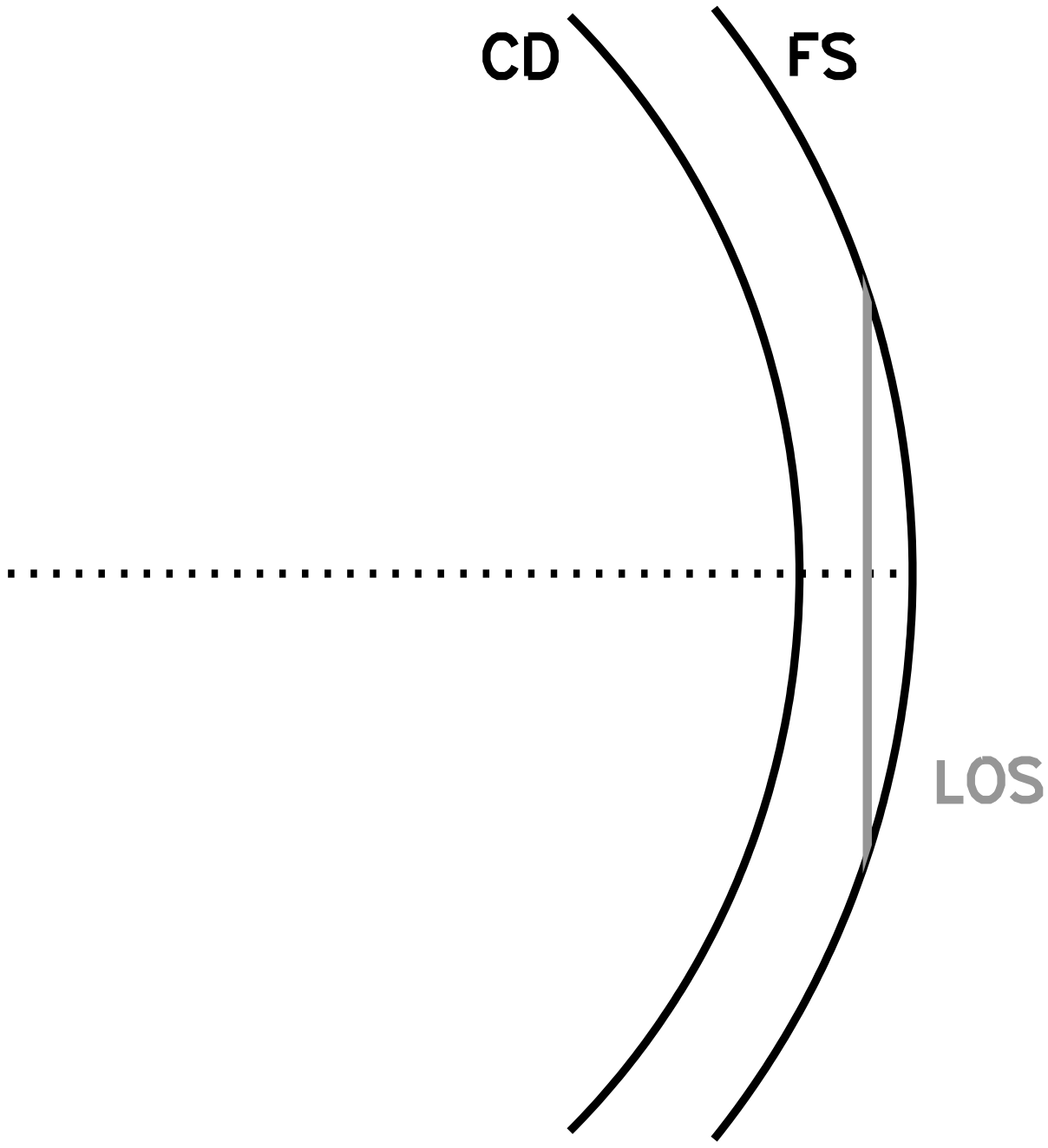

Fig. 1.— Sketch of the geometry. We discuss the transport of polarized radiation for a line of sight (LOS) near the rim of the SNR, right behind the forward shock (FS) but outside the contact discontinuity (CD).

orientation of the perpendicular component of the magnetic field at the location of the electron. It is therefore practical to directly calculate the magnetic-polarization angle, which can be compared with radio polarimetry data, for which the 90°-rotation has already been performed.

It is useful to describe polarized emission using a complex polarized intensity (Burn 1966)

$$P_\nu = I_\nu \, \exp\left(2\,\imath\,\chi\right) \ , \tag{12}$$

the phase of which is twice the magnetic-polarization angle, χ. The factor 2 in the argument of the exponential accounts for the indistinguishability of polarization angles χ and $\chi + \pi$. The complex emissivity is then similarly defined as

$$\epsilon_\nu = p\, j_\nu \, \exp\left(2\,\imath\,\psi\right) \ , \tag{13}$$

where the initial magnetic-polarization angle, ψ, reflects the orientation of the magnetic field perpendicular to the line of sight through the relations

$$\cos\psi = \frac{B_{x'}}{B_\perp} \qquad \sin\psi = \frac{B_{y'}}{B_\perp}. \tag{14}$$

Polarized radio emission will suffer Faraday rotation upon passage through a magnetized plasma. The amount of rotation is proportional to the square of the wavelength, and the proportionality constant is usually defined as the Faraday depth of the source. The final polarization angle

$$\chi(\lambda^2) = \psi + \phi\lambda^2, \tag{15}$$

where ϕ is the Faraday depth calculated as a pathlength integral along the line of sight of the local electron plasma frequency, $\omega_{p,e}$, the electron gyrofrequency, ω_g, and the inclination angle between the line of sight and the magnetic-field vector, ξ (Burn 1966; Brentjens & de Bruyn 2005).

$$\phi(s) = \frac{-1}{4\pi^2\,c^3} \int_0^s ds'\,\omega_{p,e}^2\,\omega_g\,\cos\xi = \left(0.81\ \mathrm{rad\,m^{-2}}\right) \int_0^s \left(\frac{n_e}{\mathrm{cm^{-3}}}\right)\left(\frac{B_{\rm los}}{\mu\mathrm{G}}\right)\left(\frac{ds'}{\mathrm{pc}}\right) \tag{16}$$

Also, n_e denotes the density of free electrons and $B_{\rm los} = B_{z'}$ is the magnetic-field component along the line of sight (positive when pointing toward the observer). In the absence of absorption the transport of polarized radio emission is then given by line-of-sight integration.

$$\begin{aligned} P_\nu &= \int_0^{L_{\rm LOS}} \epsilon_\nu(s)\,\exp\left[2\imath\,\phi(s)\lambda^2\right] ds \\ &= \int_0^{L_{\rm LOS}} p\ j_\nu(s)\,\exp\left[2\imath\ \left(\phi(s)\lambda^2 + \psi(s)\right)\right] ds \end{aligned} \tag{17}$$

where $L_{\rm LOS}$ is the length of the line of sight, here 20,000 cells. We calculate the observed degree of polarization as

$$\Pi_\nu = \frac{|P_\nu|}{I_\nu} = \frac{|\int ds\ p\, j_\nu(s)\ \exp\left[2\imath\ (\phi(s)\lambda^2 + \psi(s))\right]|}{\int ds\ j_\nu(s)} \tag{18}$$

and the observed polarization angle according to Eq. 12.

It is worth noting three particular aspects of our method.

1. The degree of polarization does not depend on the rms amplitude of the perpendicular component of the magnetic field, only on the spatial fluctuations and the orientation. It also does not depend on the spectral index, if we ignore the minimal variation of the intrinsic degree of polarization, p (cf. eq. 11). In the absence of Faraday rotation, i.e. if $|\phi(s)|\lambda^2 \ll \pi$, also the line-of-sight component of the magnetic field, $B_{\rm los}$, cancels out of Eq. 18, which is then solely dependent on the structure of the turbulent field. The frequency cancels as well, and therefore we will find that at high frequencies the degree of polarization is inevitably small, if the magnetic field is fully and isotropically turbulent on small spatial scales. A significant homogeneous field or anisotropy of the turbulence, e.g. through shock compression, will increase the polarization fraction.

2. Faraday rotation will generally lead to additional depolarization, if $|\phi(s)|\lambda^2 \gtrsim \pi$. Our examples assume numerical values of $n_e = 1\,{\rm cm}^{-3}$, a line-of-sight length $L_{\rm LOS} = 10\,{\rm pc}$, and a mean turbulent magnetic-field strength of $\delta B \approx 10\mu$G for the Kolmogorov models and $\delta B \approx 20\mu$G for the flat-spectrum models. Variations in one variable can be fully compensated by variation in another variable, in particular the wavelength λ. Faraday rotation may simply become important at somewhat higher (or smaller) frequency than shown in our figures. Because of the quadratic wavelength dependence, relatively small changes in wavelength can compensate for relatively large changes in the other variables.

3. We have described the radiation transport along a single line of sight. Since we simulate a grid of 20x20x20000 cells or 50x50x20000 cells, we can also account for beam depolarization for a beam size of 20x20 or 50x50 cells, respectively. This beamsize corresponds to a linear resolution of 0.1% or 0.25% of the line-of-sight length. $L_{\rm LOS}$ is typically a fair fraction of the SNR radius (see Fig. 1), and hence our beam size corresponds to somewhat less than 0.1% of the angular radius of the SNR. Most published radio observations have larger beams, and thus we underestimate the beam depolarization.

3. Results

3.1. Isotropic strong turbulence

The most generic case to consider is isotropic turbulence without a large-scale homogeneous magnetic-field component. The calculations should broadly describe situations in which $\delta B \gg B_0$, as is often invoked for young SNRs. Figure 2 shows the degree of polarization as a function of frequency for a selection of magnetic-field models with Kolmogorov and flat turbulence spectra. In all cases the polarized intensity was "beam-integrated" over an area of 20 by 20 cells. We find the behavior of polarized radio-synchrotron emission well characterized by the following statements:

- Generally, magnetic-field models based on a Kolmogorov turbulence spectrum tend to give a higher polarization degree than models for flat turbulence spectra. This behavior can be understood with a toy model, in which the magnetic field is assumed constant in a zone of "wavelength" l, but having random variations from zone to zone. If there are N zones on the line of sight, the mean observed degree of polarization would be about $70\%/\sqrt{N}$. For the Kolmogorov models we find an observed degree of polarization around 8%, or $N = 80$, or $l \simeq 250$ cells. For flat-spectrum turbulence, which has much higher amplitudes at small scales, we find 4%, or $N = 300$, or $l \simeq 65$ cells. We can extrapolate to turbulence of smaller wavelength than simulated here, for which we expect the observed degree of polarization to be less than 4% on average.

- The observed polarization angles are uniformly distributed on scales larger than the characteristic wavelength of the turbulence, which is easily understood in the framework of the toy model described under the first bullet above. Because our turbulence model is built through the superposition of waves, two lines of sight close to each other will pass through magnetic-field structures that are somewhat correlated, whereas lines of sight far from each other will be fully uncorrelated.

- Figure 3 shows the small-scale distribution of the observed magnetic-polarization angle at 4.8 GHz for a Kolmogorov model. To be noted from the figure is that the polarization angle varies by less than 0.3 radian over an area of 50x50 cells, whereas it varies wildly over significantly larger areas. Therefore, the beam depolarization is small, if we beam-integrate the polarized intensity only over the 50x50 cells, or 20x20 cells as done for Fig. 2. Real radio measurements have a spatial resolution that is much worse than 0.25% of the line-of-sight length (50 cells vs. 20,000 cells). Therefore, beam depolarization may be much more significant in the real data, and the observed polarization degree may be lower than shown in Fig. 2.

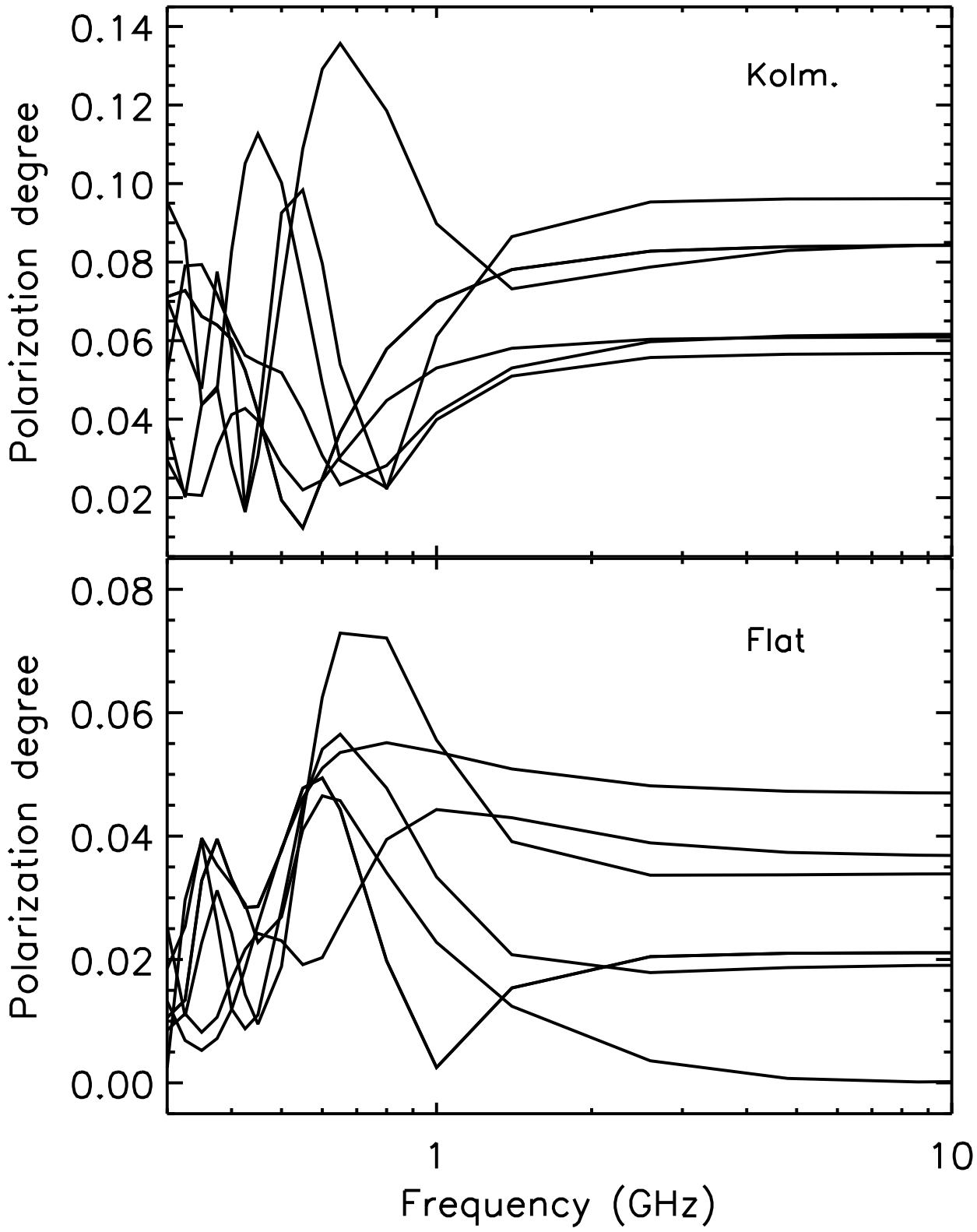

Fig. 2.— The degree of polarization as a function of frequency for a selection of six turbulence models assuming Kolmogorov spectra (top panel) and six models based on flat spectra (bottom panel).

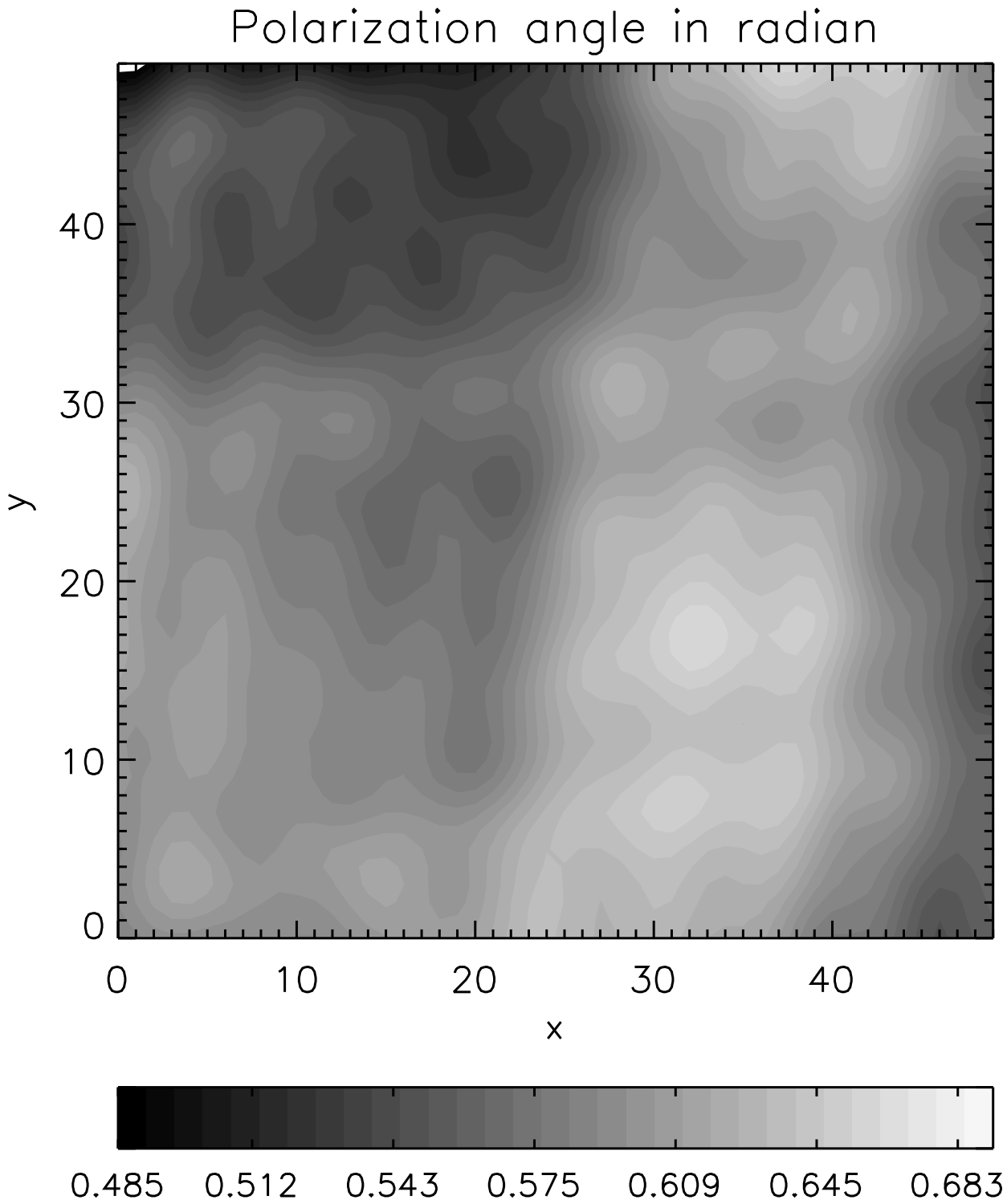

Fig. 3.— The spatial variation of the observed magnetic polarization angle at 4.8 GHz, where internal Faraday rotation is negligible. A turbulence model with Kolmogorov spectrum was chosen. The plot covers a surface area of 50x50 cells, while the line of sight is 20,000 cells long.

- At higher frequencies the observed polarization degree is determined only by depolarization through the intrinsic magnetic-polarization angle, ψ, which reflects the orientation of the perpendicular magnetic-field component along the line-of-sight (cf. Eq. 14).

- In Fig. 2 we see substantial fluctuations in the degree of polarization between different magnetic-field models with the same turbulence spectrum. We expect that for a wider beam much of this variation would be smoothed out.

- Below about 1 GHz Faraday rotation becomes important. If the product of rms magnetic-field strength, δB, free-electron density, n_e, and line-of-sight length, $L_{\rm LOS}$, in any SNR is different from the canonical values described in Sec. 2.2, then the onset of Faraday depolarization may occur at a somewhat lower or higher frequency.

- Because the magnetic field is turbulent, the effective Faraday rotation in the observed polarization angle no longer follows a λ^2-law (Brentjens & de Bruyn 2005). Faraday rotation in the foreground – not considered here – will follow the λ^2-dependency, but it generally cannot be extracted using a λ^2-law because it is superimposed on the internal Faraday rotation.

- The strong Faraday rotation at low frequencies reduces the polarization degree only weakly, because the polarized emissivities are already fully randomized at high frequency.

3.2. Mixtures of turbulent and homogeneous fields

The magnetic field near the rim of SNRs may not be fully turbulent, for example if the magnetic-field amplification saturates at an amplitude $\delta B \approx B_0$. We can model a mixture of turbulent and homogeneous fields by adding to our models of fully turbulent magnetic field a homogeneous field that is oriented in the x-direction.

In Fig. 4 we show the degree of polarization as a function of frequency for mixtures of turbulent and homogeneous fields of varying strength. The polarized intensity has been "beam-averaged" over 50x50 cells, or 0.25% of the line-of-sight length, and therefore the curve for a fully turbulent field is smoother at low frequency compared with those shown in Fig. 2.

Largely independent of the choice of turbulence model, a homogeneous magnetic field of the same strength as the rms turbulence amplitude, $B_0 = \delta B$, drives the degree of polarization into the range 30% to 35%. A homogeneous magnetic field at $B_0 = 2\,\delta B$ gives a degree of polarization at the level 55% to 60%. However, at low frequencies where internal Faraday

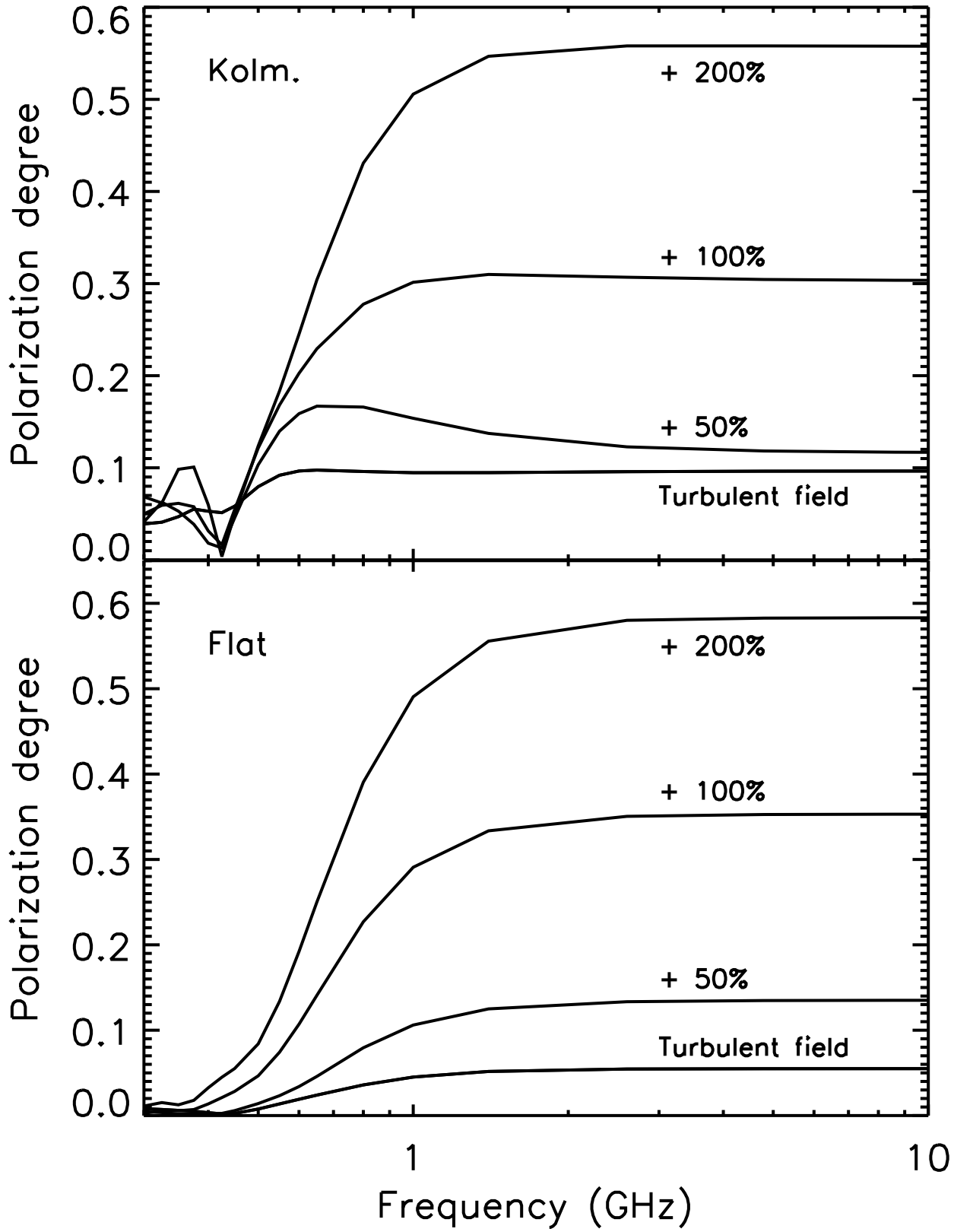

Fig. 4.— The observed polarization degree as a function of frequency for models with a homogeneous field component of varying strength (50%, 100%, or 200% of the rms turbulence amplitude, δB). The top panel shows results for Kolmogorov turbulence, and the lower panel displays the degree of polarization in the case of turbulence with flat spectrum.

Model	Turb. only	+50%	+100%	+200%
Flat_01	40.59	8.42	4.21	2.58
Flat_02	0.43	1.92	1.20	0.81
Klm_01	35.59	22.52	5.67	1.85
Klm_02	87.57	12.84	4.13	2.43

Table 1: Magnetic polarization angles, given in degrees relative to the direction of the homogeneous field ($B_0\,\mathbf{e_x}$), for varying ratios $B_0/(\delta B)$ and a selection of turbulence models. The frequency is 4.8 GHz, and so internal Faraday rotation is very small.

rotation is important the degree of polarization remains below 10%, and for flat-spectrum models, i.e. a very small effective turbulence wavelength, the polarization degree falls below 3%.

Table 1 gives the observed magnetic-polarization angles at high frequency for different relative amplitudes of the homogeneous field, which is oriented in the x-direction (zero angle). Recall that the magnetic-polarization angle differs by 90° from the electric polarization angle. Already for $B_0 = \delta B$ the magnetic-polarization angles reflect the direction of the homogeneous field component to within a few degrees. At low frequencies, where internal Faraday rotation is strong, two lines of sight through statistically independent turbulence give a different polarization angle as if randomly selected, irrespective of the magnitude of the homogeneous field, but the degree of polarization is small.

3.3. Shock-compressed turbulence

If strong magnetic turbulence is generated upstream of the shock, for example by the streaming of cosmic rays (Bell 2004), then it will change its properties when transmitted through the shock. Here we investigate this situation for the simplified case that the modification by the shock can be fully described by a compression of the spatial scales in the direction of the shock normal (here the x-axis) and an increase of the perpendicular magnetic-field components. The change in spatial scale is achieved by reallocating the gridpoints of the mesh on which the magnetic field is calculated (see sec. 2.1). Instead of sampling with $\Delta x = \Delta y = \Delta z$ the magnetic-field model is interpreted as sampled with $\Delta x = (\Delta y)/\kappa$ where κ is the compression ratio. The compression of the perpendicular field components is effected by the substitution $B_y \longrightarrow \kappa\, B_y$ and likewise for B_z.

In Fig. 5 we show the polarization degree as a function of frequency for shock compres-

Model	Turb. only	$\kappa = 2$	$\kappa = 3$
Flat_01	40.59	91.42	93.48
Flat_02	0.43	91.84	92.63
Klm_01	35.59	85.66	89.46
Klm_02	87.57	92.48	93.72

Table 2: Magnetic polarization angles, given in degrees relative to the shock normal, for varying compression ratios and a selection of turbulence models. The frequency is 4.8 GHz, and so internal Faraday rotation is very small.

sion with $\kappa = 2$ and $\kappa = 3$, where the "beam-averaging" is effectively over 20x20 and 15x15 cells, respectively, so the "beamsize" decreases with increasing κ. Cosmic rays can modify the shocks at which they are accelerated, resulting in a reduction of the compression ratio at the subshock of the thermal gas and an increase in the overall compression (Reynolds 2008). The choice of compression ratios in figure 5 is solely meant to illustrate the behavior of the polarization, and in fact the changes in the degree of polarization will be only more pronounced for larger compression ratios. To be noted from the figure is that shock compression will substantially increase the degree of polarization at higher frequencies: already for a compression ratio $\kappa = 2$ the degree of polarization falls into the range 35% to 40%, largely independent of the choice of turbulence model. As in the case of a mixture with a homogeneous field, Faraday rotation will strongly depolarize the emission at low frequency. The onset of efficient internal Faraday rotation is observed at somewhat higher frequency than in the case of a homogeneous field component perpendicular to the line of sight, because the shock compression also increases the line-of-sight component of the magnetic field and hence the Faraday depth. While shock compression or a homogeneous field component can increase the degree of polarization, they will inevitably also modify the observed magnetic-polarization angle which is shown in Table 2. Even for a moderate compression ratio $\kappa = 2$, at high radio frequencies the magnetic-polarization angles lie around 90° to the shock normal with very little scatter (the electric polarization is along the shock normal). At low frequencies Faraday rotation randomizes the polarization angle, but the degree of polarization is generally small. We can conclude that shock compression will not give a high degree of polarization $\gtrsim 20\%$ *and* a magnetic polarization aligned with the shock normal.

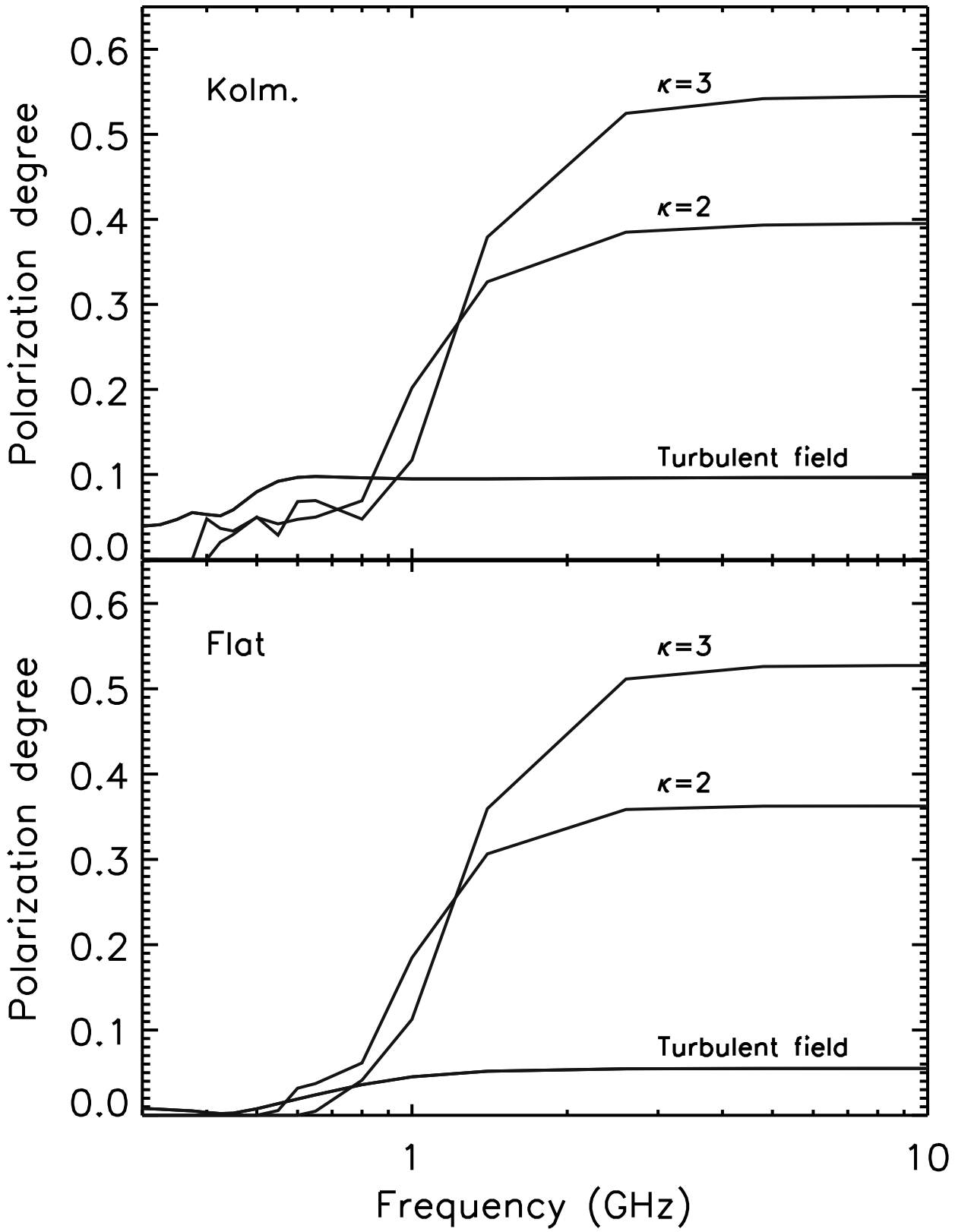

Fig. 5.— The observed polarization degree as a function of frequency for models with shock-compressed turbulence for a choice of compression ratios, κ. The top panel shows results for Kolmogorov turbulence, and the lower panel displays the degree of polarization in the case of turbulence with flat spectrum.

4. Discussion and summary

We have seen that isotropic strong turbulence will produce weakly polarized radio emission even in the absence of internal Faraday rotation. The polarization angle can be expected to vary on spatial scales of the order of the typical wavelength of the magnetic-field fluctuations, and therefore radio polarimetry data of very high angular resolution are needed to observe those variations.

If anisotropy is imposed on the magnetic-field structure, the degree of polarization can be significantly increased, provided internal Faraday rotation is inefficient. Both for shock compression and a mixture with a homogeneous field the increase in polarization degree goes along with an alignment of the observed magnetic-polarization angle with the direction of the dominant magnetic-field components. In the case of shock compression we therefore expect tangential magnetic polarization at the rims of SNRs, or electric polarization vectors that are predominantly radial in orientation.

Few young SNRs are suitable for the study of strong magnetic turbulence through radio polarimetry. Some remnants like Cas A feature ejecta beyond the nominal forward shock (Hwang et al. 2004), and therefore our assumption of a simple, spherically symmetric structure does not apply. Also, the line-of-sight should not pass through the contact discontinuity, at which the magnetic field may be very strong (Rosenau & Frankenthal 1976; Lyutikov & Pohl 2004). It is well known that the contact discontinuity is hydrodynamically unstable (e.g. Blondin & Ellison 2001), and so in projection it will appear as an extended feature with a turbulent field structure. Also, if the SNR efficiently accelerates cosmic rays, the contact discontinuity will be closer to the forward shock than in a purely hydrodynamical SNR. Using X-ray measurements, Warren et al. (2005) on average find traces of the contact discontinuity in Tycho's SNR out to 93% of the projected radius of the forward shock. Cassam-Chenaï et al. (2008) use the same technique on data of the remnant of SN 1006 and find that in the regions of bright non-thermal X-ray emission the contact discontinuity extends all the way to the forward shock. In both remnants the proximity of forward shock and the contact discontinuity presumably arises from a combination of hydrodynamical instabilities of the contact discontinuity and structural modifications on account of cosmic-ray acceleration. In any case, in SN 1006 we may not find a line of sight that is clearly inside the forward shock but outside the contact discontinuity. For Tycho's SNR radio-polarimetry data are required with an angular resolution around 1% of the angular radius, so the forward shock and the contact discontinuity are at least a few beamwidth apart.

DeLaney et al. (2002) observed the polarized synchrotron emission from Kepler's SNR at 6 cm and 20 cm wavelength. After rotating the measured electric polarization by 90°, they found predominantly radial magnetic polarization in the outer regions of the remnant,

where the degree of polarization was a few per cent at 6 cm and less than that at 20 cm. The angular resolution is moderate, though, and the beam size is about 7% of the projected radius of the forward shock. This is a factor of 100 worse than the beamsize assumed for the figures in this paper, and a direct comparison is therefore difficult. Also, the contact discontinuity and the forward shock are not clearly separated at this resolution, and so any inferred field orientation and turbulence level cannot be unambiguously associated with the magnetic-field structure directly behind the forward shock.

Dickel et al. (1991) presented radio polarimetry data of Tycho's SNR at 6 cm and 20 cm wavelength. The spatial resolution is about 0.7% of the forward-shock radius, roughly comparable to 300 cells in our magnetic-field model. The radio morphology can be well described by an outer rim and an inner shell of outer radius 0.92 SNR radii (Katz-Stone et al. 2000). The outer rim is positionally coincident with the outer periphery of the X-ray emission, suggesting that the inner shell marks the location of the contact discontinuity and the reverse shock. We conclude that our model is applicable to polarized radio emission from the outer rim.

In the outer rims, the percentage polarization at 6 cm wavelength is typically in the range 20% to 30%, and the field orientation is radial (cf. Fig.5a of Dickel et al. 1991). Beginning about $10''$(or 7% of the SNR radius) toward the interior of the remnant, the degree of polarization is lower and the polarization angle varies on scales of about $10''$, consistent with large scale turbulence near the contact discontinuity. Internal Faraday rotation is likely negligible, because no deviation from a λ^2-law is observed between 6 cm and 20 cm. The lack of efficient internal Faraday rotation can be used to set limits on the amplitude of the turbulent magnetic field. The post-shock gas density in Tycho is not well known, but the estimates include our canonical number $n_e = 1$ cm^{-3}. The distance is likely in the range 1.5 kpc to 3 kpc (Smith et al. 1991), and therefore the line-of-sight length at the rim is $L_{\rm LOS} \approx 0.5$ pc. For the canonical numbers used in our model internal Faraday rotation becomes important at about 1 GHz, which with the gas density and physical size of Tycho's SNR requires $\delta B \simeq 200$ μG. If the field strength were significantly larger than that, Dickel et al. (1991) should have observed internal Faraday rotation.

Comparing with our model results presented in Sec. 3, we find no evidence for isotropic or shock-compressed magnetic turbulence that is amplified to an amplitude larger than the homogeneous magnetic field. The radio data are compatible with two scenarios: a turbulent magnetic field superimposed on a radial large-scale field of similar amplitude, i.e. a parallel forward shock with $\delta B \simeq B_0$, or, alternatively, anisotropic turbulence that has a somewhat larger magnetic-field amplitude in the radial direction.

Anisotropic magnetic turbulence with preferentially radial orientation is not expected

in models involving magnetic-field amplification by streaming cosmic rays in the upstream region, in particular on account of shock compression. We note with interest that recent MHD simulations of magnetic-field growth following shock distortions on account of density fluctuations in the upstream medium suggest that the radial magnetic-field components may be slightly stronger than those in the shock plane (Zirakashvili & Ptuskin 2008). Additional simulations with higher resolution are needed to confirm these findings and establish their dependence on the wavelength of the density fluctuations and other parameters (e.g. Cho et al. 2008).

We acknowledge support by NASA under award No. NAG5-13559.

REFERENCES

Balsara, D., Benjamin, R.A., Cox, D.P. 2001, ApJ 563, 800

Bamba, A., Yamazaki R., Yoshida T., Terasawa T., Koyama K. 2005, ApJ 621, 793

Bamba, A., Yamazaki R., Ueno M., Koyama K. 2003, ApJ 589, 827

Bell, A.R. 2005, MNRAS 358, 181

Bell, A.R. 2004, MNRAS 353, 550

Bell, A.R. 1978, MNRAS 182, 442

Bell, A.R., Lucek, S.G. 2001, MNRAS 321, 433

Blondin, J.M., Ellison, D.C. 2001, ApJ 560, 244

Brentjens, M.A., de Bruyn, A.G. 2005, A&A 441, 1217

Burn, B.J. 1966, MNRAS 133, 67

Butt, Y., Porter, T.A., Katz, B., Waxman, E. 2008, MNRAS 386, L20

Bykov, A.M., Uvarov, Y.A., Ellison, D.C. 2008, ApJL 689, 133

Bykov, A.M., Toptygin, I.N. 2005, Astron. Lett. 31-11, 748

Cassam-Chenaï, G., Hughes, J.P., Reynoso, E.M., Badenes, C., Moffett, D. 2008, ApJ 680, 1180

Cho, J., Vishniac, E.T., Beresnyak, A., Lazarian, A., Ryu, D., 2008, ApJ in press, (arXiv:0812.0817)

Cho, J., Lazarian, A., 2002, ApJL 575, 63

DeLaney, T., Koralesky, B., Rudnick, L., Dickel, J.R. 2002, ApJ 580, 914

Dickel, J.R., van Breugel, W.J.M., Strom, R.G. 1991, AJ 101, 2151

Giacalone J. 2005, ApJ 624, 765

Giacalone J., Jokipii, J.R. 2007, ApJL 663, 41

Giacalone J., Jokipii, J.R. 1996, JGR 101, 11095

Giacalone J., Jokipii, J.R. 1994, ApJL 430, 137

Ginzburg, V.L., Syrovatskii, S.I. 1964, *The origin of cosmic rays*, New York: Macmillan

Gotthelf, E.V., et al. 2001, ApJL 552, 39

Green, D.A., 2001, in *High energy gamma-ray astronomy*, eds. F.A. Aharonian and H.J. Völk, AIP Conference Proceeding 558, 59

Huang, C.-Y., Pohl, M. 2008, Astropart. Phys. 29, 282

Hughes, J.P. 2000, ApJL 545, 53

Hwang, U., et al. 2004, ApJL 615, 117

Hwang, U., et al. 2002, ApJ 581, 1101

Katz, B., Waxman, E. 2008, JCAP 01, 018

Katz-Stone, D.M., Kassim, N.E., Lazio, T.J.W., and O'Donnell, R. 2000, ApJ 529, 453

Lagage, P.O., Cesarsky, C. 1983, A&A 125, 249

Lagage, P.O., Cesarsky, C. 1983, A&A 118, 223

Le Roux, E. 1961, Ann. d'Astroph. 24, 71

Lucek, S.G., Bell, A.R. 2000, MNRAS 314, 65

Lyutikov, M., Pohl, M. 2004, ApJ 609, 785

Malkov, M.A., Diamond, P.H. 2001, Phys. Plasmas 8 (5), 2401

Niemiec, J., Pohl, M., Stroman, T., Nishikawa, K.-I. 2008, ApJ 684, 1174

Niemiec, J., Ostrowski, M. 2006, ApJ 641, 984

Pohl, M., Yan, H., Lazarian, A. 2005, ApJL 626, 101

Reville, B., O'Sullivan, S., Duffy, P., & Kirk, J. G. 2008, MNRAS, 386, 509

Reynolds, S.P. 2008, ARA&A 46, 89

Rosenau, P. & Frankenthal, S., 1976, Phys. Fluids, 19, 1889

Rybicki, G.B., Lightman, A.P. 1979, *Radiative Processes in Astrophysics*, Wiley Interscience, New York

Smith, R. C., Kirshner, R. P., Blair, W. P., and Winkler, P. F. 1991, ApJ, 375, 652

Uchiyama, Y., et al. 2007, Nature 449, 576

Vink, J., Laming, J.M. 2003, ApJ 584, 758

Vladimirov, A., Ellison, D.C., Bykov, A. 2006, ApJ, 652, 1246

Warren, J.S., et al. 2005, ApJ 634, 376

Zirakashvili, V.N., Ptuskin, V.S. 2008, ApJ 678, 939

Zirakashvili, V.N., Ptuskin, V.S., Völk, H.J. 2008, ApJ 678, 255

This preprint was prepared with the AAS LaTeX macros v5.2.